Heliyon 82 (2022) e10631

Contents lists available at ScienceDirect

Heliyon

journal homepage: www.cell.com/heliyon

Research article

Synthesis and characterization of MnO_2/Eggplant carbon composite for enhanced supercapacitors

X. Wang [a,*], J. Chu [b], H.J. Yan [a], H.K. Zhang [a]

[a] Department of Food Engineering, Chemistry, Harbin University, Heilongjiang, 150086, Harbin, PR China
[b] College of Chemistry and Chemical Engineering, Xi'an University of Science and Technology, 710054, Xi'an, PR China

ARTICLE INFO

Keywords:
MnO_2
Eggplant carbon
Hydrothermal
Supercapacitor

ABSTRACT

In this paper, the eggplant carbon (EC)was derived from eggplant skin by one-step carbonization method. Subsequently, the MnO_2/eggplant carbon (MnO_2/EC) composite was prepared via*in-situ* hydrothermal method. The morphology and structure as well as electrochemical performance were investigated through a series of characterization and tests. The results showed that the urchin shaped structures of MnO_2 was successfully loaded on the surface of EC. The electrochemical studies indicated that the specific capacitance of the MnO_2/ECcomposite could reach 652.5F/g at 0.5 A/g in 1 M Na_2SO_4 aqueous electrolyte. In addition, the MnO_2/EC composite exhibits excellent cyclic stability after 10000 cycles, which might be ascribed to the synergistic effect of MnO_2 and EC for the improvement of electrochemical performance. Taken together, this work demonstrated that MnO_2/EC composite can be used in the aspect of energy storage for high-performance supercapacitors.

1. Introduction

Over the past decades, in face of the excessive consumption of fossil energy and increasingly severe energy supply as well as environment pollution problem, developing sustainable and ecofriendly energy have become very urgent [1, 2, 3]. As the next-generation energy storage device, supercapacitors have much higher energy storage capacity and power density than traditional physical capacitors [4, 5, 6]. As is well known, the pseudo capacitor store charges via the redox process, which can provide a higher energy density in the faster charge-discharge than electrical double-layer capacitor (EDLC) [7, 8, 9].

The electrode materials of supercapacitors play an important role in the energy storage [10, 11]. At present, high performance electrode materials include carbon-based materials [12], transition metal oxides [13] and conductive polymers [14]. Among the various transition metal oxides, MnO_2 is an ideal charge storage material for electrochemical supercapacitors [15], because it has the advantages of high theoretical ratio (up to 1370 F/g), low cost, low toxicity and environmental friendliness [16, 17]. However, its electrical conductivity, stability and proton diffusion ability is poor, which can not meet the high-performance requirement of the supercapacitor [18, 19, 20]. In order to improve this situation, the carbon material has been used to prepare the MnO_2-based composites, which effectively improves its electrochemical performance [21, 22]. At present, carbon materials such as activated carbon, graphene and carbon nanotubes are widely used in MnO_2-based composites due to their high specific surface area, excellent electrical conductivity, unique internal structure and well thermal stability. Fu [23] reported the symmetrical supercapacitors, yielding specific capacitances of 616.3 and 481.4 F/g at 1 and 10 A/g, respectively. However, the preparation process of these carbon materials is complex and the cost is relatively high [24, 25]. Therefore, several biomass carbon materials have been developed and exhibited excellent electrochemical performance [26]. In addition, biomass carbon materials have the advantages of renewable, low cost and environmental protection [27]. Various biomass resources such as peanut shell [28], bamboo bagasse [29], sugarcane bagasse [30], egg white [31], corn silk [32], rice husk [33], pomelo peel [34] and onion [35] have been reported as the carbon precursors for supercapacitor applications. Meanwhile, the combination of biomass carbon and manganese dioxide to improve the electrochemical properties of materials has been widely studied. WU [21] obtained a two-dimensional carbon sheet composed of a large number of mesoporous and microporous structures through acid treatment and pyrolysis carbonization of cucurbit-based biomass. The specific surface area was as high as 1 308 m^2/g, and the ideal pore volume was 0.84 cm^3/g. When the current density was 1 A/g, the specific capacitance was 273 F/g. When the current density gradually increases from 1 A/g to 50

* Corresponding author.
E-mail address: wangxin5569@hrbu.edu.cn (X. Wang).

https://doi.org/10.1016/j.heliyon.2022.e10631
Received 16 March 2022; Received in revised form 1 June 2022; Accepted 8 September 2022

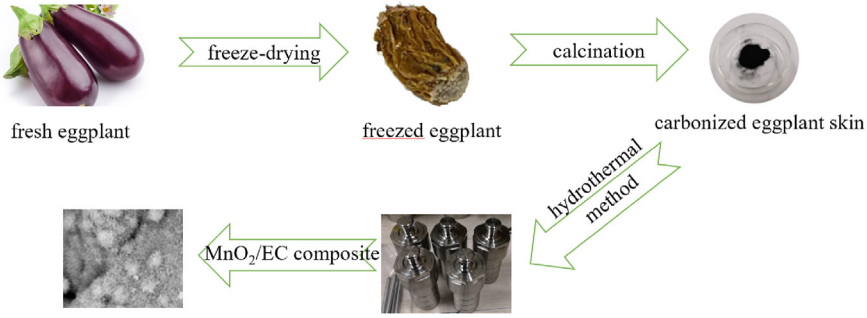

Scheme 1. Illustration of the Synthesis Process of MnO_2/EC.

A/g, the capacitance retention rate is 75 %. Liu [22] activated carbon material exhibits a high specific surface area (2490 m^2/g), and the effect of the activator addition ratio was systematically investigated. The optimized SPC-2 displayed a high specific capacitance (324 F/g at 1 A/g) and excellent cycling stability as 90.6%.

In this work, we select the eggplant skin as carbon precursor, which can be facilely converted into carbon nanosheets via simple carbonization. Then, designed a simple synthetic route for synthesis of MnO_2/EC composite utilized as the electrode material for supercapacitors. Moreover, the MnO_2/EC composite was characterized and tested by SEM, TGA and electrochemical measurement. The results showed that MnO_2/EC composite has a high specific capacitance and excellent cyclic stability, indicating this new material can be utilized in the field of energy storage.

2. Experimental method

2.1. Preparation of eggplant carbon

The fresh eggplant skin was firstly cut into small pieces. Next, the eggplant skin pieces were dried by a freeze-drying technique. Finally, the dried eggplant skin was calcined at 500 °C for 2 h in N_2 flow to obtain carbonized eggplant.

2.2. Preparation of MnO_2/EC composite

The MnO_2/EC composite was synthesized by a hydrothermal method. In a typical preparation: 3.95 g $KMnO_4$, 0.25 g eggplant carbon, 4mL H_2SO_4 and 75 mL distilled water were mixed to form a homogeneous solution under magnetic stirring. The mixture was transferred into a Teflon-lined stainless steel autoclave and maintained at 120 °C for 3 h. The product was washed with distilled water and ethanol, and then dried at 60 °C (see Scheme 1). Pure MnO_2 was also prepared in the absence of eggplant carbon using the same method described above.

2.3. Characterization

The X-ray diffraction (XRD) analysis was performed for phase characterization using a D8 ADVANCE BRUKE with Cu Kα radiation. Surface morphology was observed by Scanning electron microscope (SEM) on a Phenom/Pro. Raman spectroscopy studies were carried out using a Invia Renishaw spectrometer with an excitation wavelength of 523 nm. Fourier transform infrared spectrometry (FTIR) was studied between 4000-400 cm^{-1} on a PerkinElmer 580B spectrometer at room temperature. Thermogravimetric analysis (TGA)was carried out using a TA instrument of Mettler-Toledo TG-DSC1 HT from room temperature to 800 °C, with a heating rate of 10 °C min^{-1} under air atmosphere.

2.4. Electrochemical measurements

The cyclic voltammograms (CV) and galvanostatic charge/discharge (GCD) measurements were carried out in a three-compartment system containing 1M Na_2SO_4 as electrolyte, SCE as the reference electrode, and a Pt flake as the counter electrode. The working electrodes were fabricated as follows: First, the active material (EC, MnO_2 and MnO_2/EC)/ Carbon Black/PVDF were mixed according to the mass ratio of 80/10/10 and then dispersed in DMF for obtaining a mixed pasty electrode material. Next the pasty electrode material was coated evenly on graphite paper with the coating area of 1 × 1 cm^2. Last the active electrode was obtained after dried at 60 °C for 24 h before test. The areal loading amount of the active material on graphite paper was about 1 mg/cm^2. The CV and GCD were measured by a CHI660D electrochemical workstation with the potential window range of -0.2–0.8V. Electrochemical impendence spectroscopy (EIS) tests were conducted in the frequency range of 0.01 Hz-100kHz.

The specific capacitance of the electrodes can be calculated from the galvanostatic charging-discharging curves based on the following equation:

$$C_s = \frac{I \times \Delta t}{\Delta V \times m} \quad (1)$$

where C_s (F/g) is the specific capacitance, I(A) is the discharge current, Δt(s) is the time of galvanostatic discharge, m (g) is the mass of the active material in the electrode, andΔV (V) is the potential window [36].

3. Results and discussion

3.1. Characterization of phase structure

3.1.1. XRD analysis

The XRD patterns of the MnO_2 and MnO_2/EC composite are shown in Figure 1(a). According to the pure MnO_2 pattern, there are three major diffraction peaks appearing at 12°, 37° and 65°, which can be indexed to (001), (111) and (020) crystal face of birnessite-type MnO_2 (JCPDF No. 42–1317), respectively [38]. For the MnO_2/EC composite, the peaks appear at 12°, 37° and 65° confirming the crystal face of MnO_2 is not changed with addition of EC. Moreover, the XRD patterns of the MnO_2/EC composite shows another two broad diffraction peak near 28° and 42°, which corresponds to the carbon peak. The results confirm that the composition of EC and MnO_2under hydrothermal condition.

3.1.2. Raman analysis

The specific structure nature of the EC, MnO_2 and MnO_2/EC was investigated by the Raman spectroscopy, as shown in Figure 1(b). Typically, both EC and MnO_2/EC composite exhibit two dominant Raman peaks at 1347 cm^{-1} and 1589 cm^{-1}, which can be assigned to the D band (corresponding to the disordered carbon) and G band (corresponding to the graphitic carbon), respectively. Besides, compared with the EC sample, we can see that MnO_2 has an obvious characteristic peaks centered at 646 cm^{-1}, which can be assigned to the Mn–O lattice vibration. After the EC and MnO_2 being composited, the peak belonging to Mn–O vibrations is still observed at 646 cm^{-1} and the peaks belonging to EC are not changed.

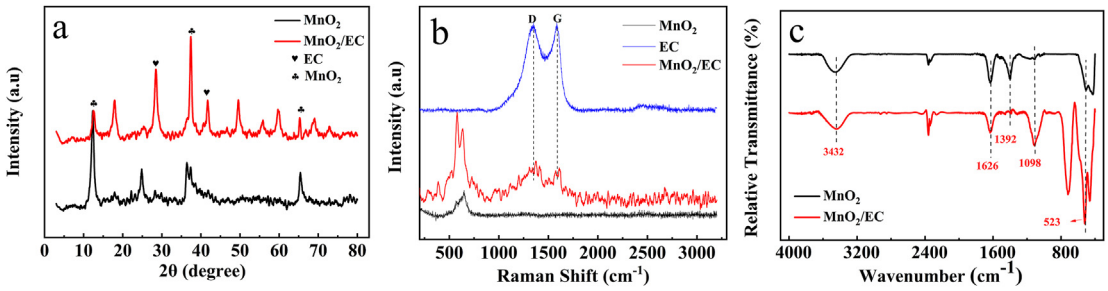

Figure 1. (a) XRD patterns of the MnO_2 and MnO_2/EC; (b) Raman spectra of the EC, MnO_2 and MnO_2/EC; (c) FTIR spectra of the MnO_2 and MnO_2/EC.

3.2. Spectroscopy analysis

Fourier transform infrared analysis was utilized to investigate the surface functional groups of MnO_2 and MnO_2/EC composite. As shown in Figure 1(c), the characteristic absorption peaks of MnO_2 appear at 523 cm^{-1}, which can be attributed to the Mn-Ovibrations, and two prominent absorption peaks at 1392 cm^{-1} and 1626 cm^{-1} correspond to the stretching vibration of O–H on Mn atom. The broad absorption bands at 3432 cm^{-1} can be assigned to the O–H stretching vibration [33]. In comparison with MnO_2, the absorption peak at 1098 cm^{-1} in the MnO_2/EC spectrum corresponds to the C–O stretching vibration. Similar vibration absorption peaks at 1626 cm^{-1} and 523 cm^{-1} are caused by the O–H stretching vibration and Mn–O bond vibration, respectively. Combined with XRD, SEM, Raman spectral and FTIR analysis, the results indicated that the MnO_2 has been successfully incorporated with EC backbone.

3.3. The surface morphology

The morphology and surface structure of the as prepared materials were characterized in terms of SEM as shown in Figure 2(a)and (b), the corrugated paper-like morphology of EC was clearly observed, which is ideal for loading the metal oxide [37]. As shown in Figure 2(c) and (d), interconnected nanorods are self-assembled to form the urchin-like architecture of MnO_2. For the MnO_2/EC composite, the urchin-like architecture of MnO_2 is well coated on EC sheets as shown in Figure 2(e) and (f). It could be expected that such an intimate interfacial contact for the MnO_2/EC would favor the electronic transport, thus leading to the improvement of the supercapacitor performance.

The TEM image of MnO_2/EC nanomaterials is shown in Figure 3(a), which further confirms the morphology of nanorods. Figure 3(b) further reveals the TEM image of MnO_2/EC at high resolution, and show that the lattice spacing of 0.357 nm for MnO_2 (002) face according to JCPDF data.

3.4. Thermal stability

The thermal stability of MnO_2 and MnO_2/EC composites were studied by TGA as shown in Figure 4. The initial weight loss of MnO_2 is 8 %, which due to the dehydration of the sample before 200 °C. A little weight loss in the range of 500–550 °C can be ascribed to the loss of oxygen in the lattice, which leads to phase transformation from MnO_2 to Mn_2O_3 [39]. TGA diagram of MnO_2/EC composite shows a slight weight loss

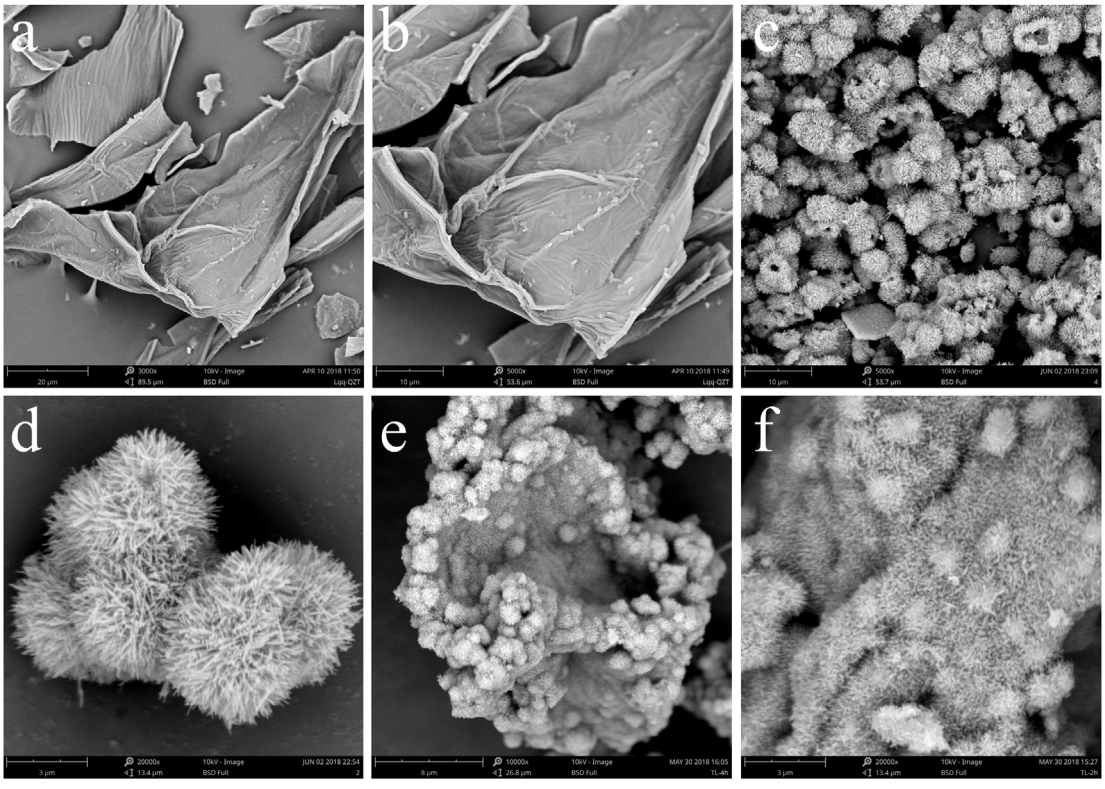

Figure 2. SEM images of EC (a, b), MnO_2 (c, d) and MnO_2/EC (e, f).

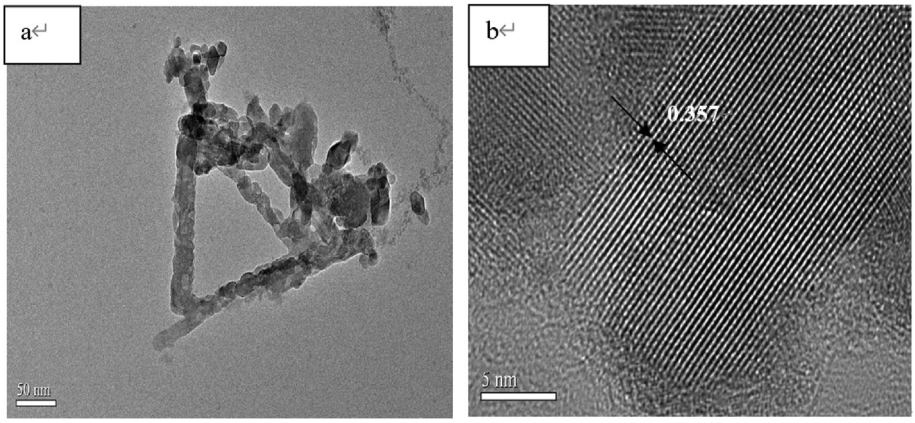

Figure 3. TEM images of MnO_2/EC (a, b).

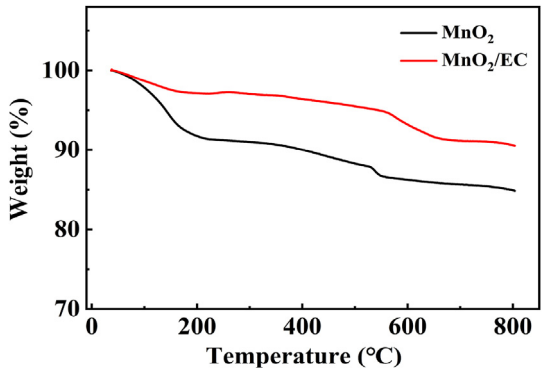

Figure 4. TGA plots of the MnO_2 and MnO_2/EC.

about 2 % when the temperature rises to 200 °C, which can be contributed to the removal of adsorbed water or crystalline hydrate [23]. In addition, the weight loss observed in the range of 200–500 °C is the combustion of carbon catalyzed by MnO_2, and with the temperature increase, residual carbon underwent combustion and the crystalline transformation of MnO_2 will occur. The results show that the stability of MnO_2/EC composite is higher than that of MnO_2.

3.5. Electrochemical properties

Figure 5 shows the electrochemical properties of the composites in a three-electrode system. The curves of CV and GCD were measured under the potential windows of -0.2–0.8 V in 1M Na_2SO_4 electrolyte. The CV curves of EC, MnO_2 and MnO_2/EC composites exhibit rectangular-like shape at a scan rate of 25 mV/s as presented in Figure 5(a). And the curves closure area of MnO_2/EC composite is much larger than pure EC and MnO_2, indicating the superior electrochemical performance of MnO_2/EC composite. This is due to the synergistic effect between EC and MnO_2 in the composite, which to some extent promotes the electrochemical performance. At the same time, the charge-discharge time of MnO_2/EC composite is longer than pure EC and MnO_2, as shown in Figure 5(b). According to Eq. (1), the C_s of the EC, MnO_2 and MnO_2/EC composite are 134.2 F/g, 400.5 F/g and 652.5 F/g at current density of 0.5 A/g, respectively. The specific capacitance of MnO_2/EC composite is nearly five times as much as that of carbon material. This means that the composites have excellent capacitance rate and high coulombic efficiency. Figure 5(c) presents the CV curves of the MnO_2/EC composites at different scan rates. With the increase of scanning rate, the shape of the curves shows some distortions from the rectangle, which may be due to the polarization of the increase of ion transport and contact resistance between electrolyte and MnO_2 [40]. Additionally, the oxidation-reduction peaks in the CV curves of the composites are not obvious, which may be due to the enhancement of the electrical conductivity of the materials after the addition of EC, and the rapid reversible conversion of manganese ions between different valence states. As shown in Figure 5(d), the GCD curves of MnO_2/EC composite at different current densities are almost symmetric with slight deformation, which illustrated the pseudocapacitive along with the electric double-layer contribution. The relationship between specific capacitance and current density are presented in Figure 5(e). The specific capacitance for all samples decreases with the increasing of current density. Significantly, the specific capacitance of MnO_2/EC composite remained 229 F/g even at a high current density of 10 A/g, this value is still larger than that of the EC and MnO_2. This result suggests that the MnO_2/EC composite possesses a high rate of capacitance, which is recognized as one of the most essential electrochemical properties for supercapacitor application.

The electrochemical properties of the EC, MnO_2 and MnO_2/EC composite were further studied by EIS as shown in Figure 5(f). The linear curve slope in the low frequency region represents the diffusion resistance of the electrolyte in the electrode surface, while the compressed semicircle in the high frequency region and the intermediate frequency region indicates the charge transfer resistance. It is obvious that in the low frequency region, the EC is an approximate vertical straight line along the virtual coordinates, which indicates its ideal double layer capacitive behavior. The semicircle diameter of MnO_2/EC is smaller than that of pure MnO_2, which indicates that the charge transfer resistance of MnO_2/EC composite is smaller than that of pure MnO_2, and the EC component of MnO_2/EC composite is favorable for electron transport. In addition, in the low frequency region, it can be seen that the slope of the composite electrode MnO_2/EC is much larger than that of pure MnO_2, which means that the MnO_2/EC has a lower diffusion resistance and a faster ion transport speed due to the introduction of the carbon material.

3.5.1. Long-term cyclic stability

The long-term cyclic stability is an important criterion in the supercapacitors applications. The cyclic stability of pure MnO_2 and MnO_2/EC was tested by repeating the constant current charge/discharge test at a current density of 0.5 A/g for 10000 cycles. As shown in Figure 6, at the first 800 cycles, the specific capacitance is decayed gradually with the test goes on, especially for MnO_2, its specific capacitance fade to 60%. After 10000 cycles, the capacitance retention rate of MnO_2 and MnO_2/EC composite is about 50 % and 79.2 %, respectively. It indicates that MnO_2/EC composite has outstanding cycle stability than pure MnO_2 [41].

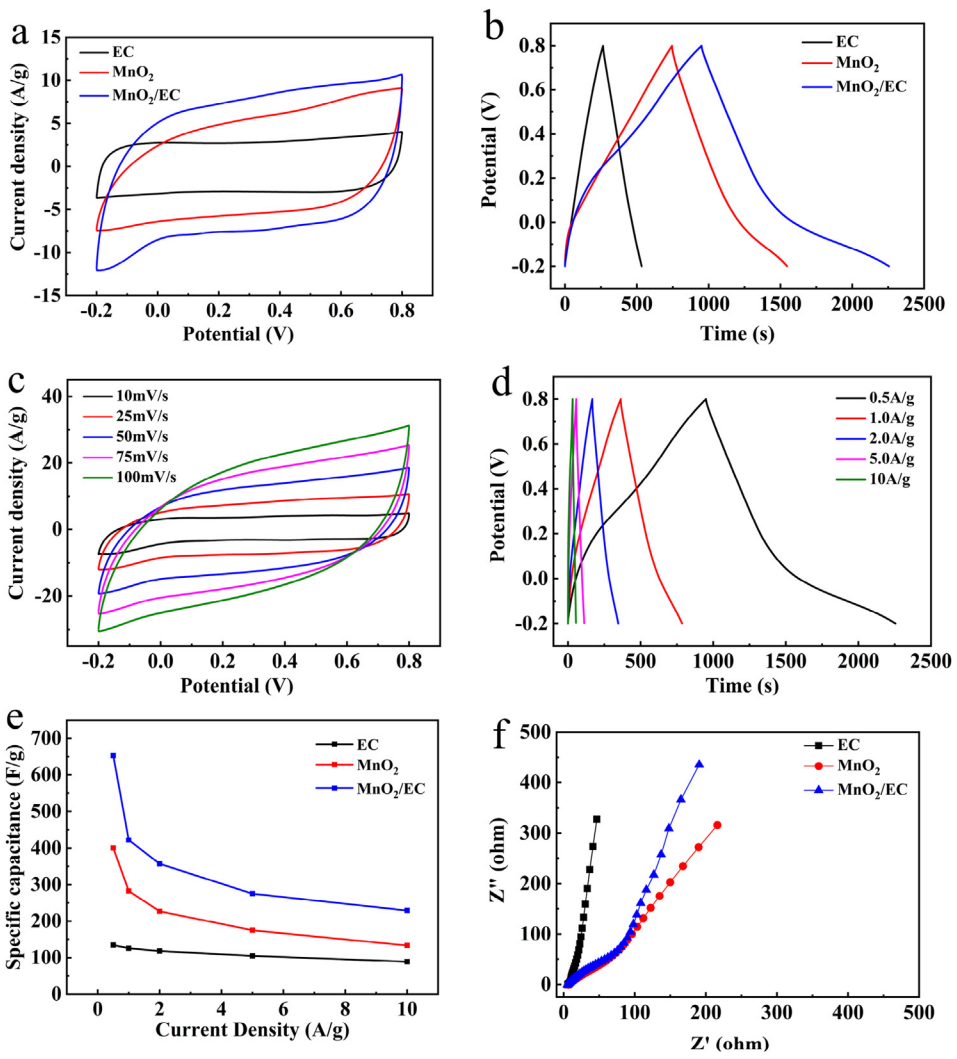

Figure 5. (a) CV curves of EC, MnO_2 and MnO_2/EC composites at 25 mV/s. (b) Galvanostatic charge/discharge curves of EC, MnO_2 and MnO_2/EC composites at 0.5 A/g. (c) CV curves of MnO_2/EC composites at 10, 25, 50, 75 and 100 mV/s. (d) Galvanostatic charge/discharge curves of MnO_2/EC composites at 0.5, 1.0, 2.0, 5.0 and 10 A/g. (e) Specific capacitance of EC, MnO_2 and MnO_2/EC composites at different current densities. (f) Electrochemical impedance spectroscopy curves of EC, MnO_2 and MnO_2/EC.

4. Conclusion

In this paper, we successfully prepared MnO_2/EC composite via*in-situ* hydrothermal method. The structure and morphology analysis show that the urchin shape MnO_2 was successfully loaded on the fold of the EC surface. The results of electrochemical measurement show that the specific capacitance of MnO_2/EC composite remain 652.5 F/g at 0.5 A/g with a higher cycling stability of 79.2 % after 10000 charge and discharge cycles. This is due to the synergistic effect of MnO_2 and EC, in which MnO_2 provides a higher pseudo-capacitance and EC enhances the overall conductivity of the material, so that the composite has excellent capacitance performance. It is believed that biomass carbon as electrode material has a broad application prospect in new carbon-based composite supercapacitors.

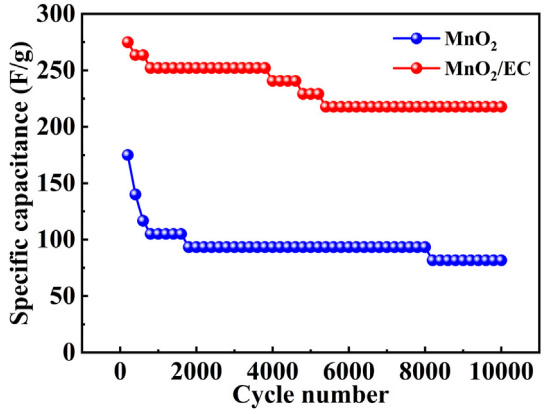

Figure 6. Cycling stability of MnO_2 and MnO_2/EC during 10000 charge-discharge cycles at 0.5 A/g.

Declarations

Author contribution statement

Xin Wang: Conceived and designed the experiments; Wrote the paper.
Jia Chu: Performed the experiments.
Huijun Yan: Analyzed and interpreted the data.
Hongkun Zhang: Contributed reagents, materials, analysis tools or data.

Funding statement

This work was supported by the Joint Guidance Project of Heilongjiang Provincial Natural Science Fund.

Data availability statement

Data included in article/supplementary material/referenced in article.

Declaration of interests statement

The authors declare no conflict of interest.

Additional information

No additional information is available for this paper.

References

[1] I. Boumanchar, K. Charafeddine, Y. Chhiti, F.E.M. Alaoui, A. Sahibed-dine, F. Bentiss, C. Jama, M. Bensitel, Biomass higher heating value prediction from ultimate analysis using multiple regression and genetic programming, Biomass Convers Bior 9 (2019) 499–509.

[2] Y. Guo, L. Zhang, Y. Liu, S. Guo, Almond shell-derived carbons under low-temperature activation with ultra-high surface area and superior performance for supercapacitors, Chemistry Select 4 (2019) 12472–12478.

[3] C. Wang, X. Liang, Z. Wang, Y. Liu, P. Wang, X. Qin, X. Zhang, Y. Dai, Y. Li, B. Huang, Vanadium nitride/porous carbon composites on Ni foam for high-performance supercapacitance, Chemistry Select 4 (2019) 11189–11195.

[4] D. Gao, Z. Luo, C. Liu, S. Fan, A Survey of Hybrid Energy Devices Based on Supercapacitors, Green Energy & Environment.

[5] Y. Jiang, X. Cui, L. Zu, Z. Hu, J. Gan, H. Lian, Y. Liu, G. Xing, Preparation and electrochemical properties of mesoporous manganese dioxide-based composite electrode for supercapacitor, J. Nanosci. Nanotechnol. 17 (2017) 507–516.

[6] Mehdi Shahedi Asl, Raha Hadi, Laleh Salehghadimi, Flexible all-solid-state supercapacitors with high capacitance, long cycle life, and wide operational potential window: recent progress and future perspectives, J. Energy Storage 50 (2022), 104223.

[7] S. Rawal, B. Joshi, Y. Kumar, Synthesis and characterization of activated carbon from the biomass of saccharum bengalense for electrochemical supercapacitors, J. Energy Storage 20 (2018) 418–426.

[8] Q. Chen, J. Chen, Y. Zhou, C. Song, Q. Tian, J. Xu, C.P. Wong, Enhancing pseudocapacitive kinetics of nanostructured MnO2 through a nchoring onto biomass-derived porous carbon, Appl. Surf. Sci. 440 (2018) 1027–1036.

[9] D. Chen, L. Yang, J. Li, Q. Wu, Effect of self-doped heteroatoms in biomass-derived activated carbon for supercapacitor applications, Chemistry Select 4 (2019) 1586–1595.

[10] Karan Kamleshbhai Patela1, Tushar Singhal, Evolution and recent developments of high performance electrode material for supercapacitors, J. Energy Storage 44 (15) (2021), 103366.

[11] C. Hao, D. Liu, Z. Shen, B. Bao, S. Zhao, L. Wu, Functional biomass carbons with hierarchical porous structure for supercapacitor electrode materials, Electrochim. Acta 180 (2015) 241–251.

[12] S. Jadhav, R.S. Kalubarme, C. Terashima, B.B. Kale, V. Godbole, A. Fujishima, S.W. Gosavi, Manganese dioxide/reduced graphene oxide composite an electrode material for high-performance solid state supercapacitor, Electrochim. Acta 299 (2019) 34–44.

[13] L. Ma, X. Shen, Z. Hu, Z. Ji, K. Chen, G. Zhu, High performance supercapacitor electrode materials based on porous NiCo2O4 hexagonal nanoplates/reduced graphene oxide composites, Chem. Eng. J. 262 (2015) 980–988.

[14] W. Zhang, B. Mu, A. Wang, Halloysite nanotubes induced synthesis of carbon/manganese dioxide coaxial tubular nanocomposites as electrode materials for supercapacitors, J. Solid State Electrochem. (2015) 1257–1263.

[15] C. Wallar, D. Luo, R. Poon, I. Zhitomirsky, Manganese dioxide-carbon nanotube composite electrodes with high active mass loading for electrochemical supercapacitors, J. Mater. Sci. 52 (2017) 3687–3696.

[16] L.H. Tseng, C.H. Hsiao, D.D. Nguyen, P.Y. Hsieh, C.Y. Lee, N.H. Tai, Activated carbon sandwiched manganese dioxide/graphene ternary composites for supercapacitor electrodes, Electrochim. Acta (2018) 284–292.

[17] N. Zhang, P. Qi, Y.H. Ding, C.J. Huang, J.Y. Zhang, Y.Z. Fang, A novel reduction synthesis of the graphene/Mn3O4nanocomposite for supercapacitors, J. Solid State Chem. 237 (2016) 378–384.

[18] Z.C. Hong, Y. Shi, H. Qin, K. Su, The preparation of MnO2 hollow spheres for electrochemical capacitor, Mater. Lett. 162 (2016) 131–134.

[19] L. Zhang, S. Du, L. Yi, Z. Peng, X. Yuan, J. Huang, S. Guo, Manganese dioxide nanoflakes anchored on reduced graphene oxide with superior electrochemical performance for supercapacitors, Micro Nano Lett12 (2017) 147–150.

[20] X. Zhang, X. Meng, S. Gong, L. Ping, L.E. Jin, Q. Cao, Synthesis and characterization of 3D MnO2/carbon microtube bundle for supercapacitor electrodes, Mater. Lett. 179 (2016) 73–77.

[21] S. Liu, K. Chen, Q. Wu, et al., Ulothrix-derived sulfur-doped porous carbon for high-performance symmetric supercapacitors, ACS Omega 7 (12) (2022) 10137–10143.

[22] Q. Li, M. Liu, F. Huang, et al., Co9S8@MnO2 core–shell defective heterostructure for High-Voltage flexible supercapacitor and Zn-ion hybrid supercapacitor, Chem. Eng. J. 26 (2022) 135494.

[23] M. Fu, Z. Zhu, Z. Zhang, et al., Microwave assisted growth of MnO_2 on biomass carbon for advanced supercapacitor electrode materials, J. Mater. Sci. 56 (2021) 6987–6996.

[24] L. Guardia, L. Suarez, N. Querejeta, V. Vretenar, P. Kotrusz, V. Skakalova, T.A. Centeno, Biomass waste-carbon/reduced graphene oxide composite electrodes for enhanced supercapacitors, Electrochim. Acta 298 (2019) 910–917.

[25] Y. Li, N. Yu, Y. Peng, Y. Li, X. Zhou, S. Chen, G. Wang, W. Tong, Z. Fan, Fabrication of manganese dioxide nanoplates anchoring on biomass-derived cross-linked carbon nanosheets for high-performance asymmetric supercapacitors, J. Power Sources 300 (2015) 309–317.

[26] G. Zhang, Y. Chen, Y. Chen, H. Guo, Activated biomass carbon made from bamboo as electrode material for supercapacitors, Mater. Res. Bull. 102 (2018) 391–398.

[27] T. Rasool, V.C. Srivastava, M.N.S. Khan, Utilisation of a waste biomass, walnut shells, to produce bio-products via pyrolysis: investigation using ISO-conversional and neural network methods, Biomass Convers Bior 8 (2018) 647–657.

[28] F. Guo, X. Jiang, X. Li, K. Peng, C. Guo, Z. Rao, Carbon electrode material from peanut shell by one-step synthesis for high performance supercapacitor, J. Mater. Sci. Mater. Electron. 30 (2018) 914–925.

[29] S.S. Gunasekaran, S.K. Elumalali, T.K. Kumaresan, R. Meganathan, A. Ashok, V. Pawar, K. Vediappan, G. Ramasamy, S.Z. Karazhanov, K. Raman, R. Subashchandra Bose, Partially graphitic nanoporous activated carbon prepared from biomass for supercapacitor application, Mater. Lett. 218 (2018) 165–168.

[30] S.X. Xiong, X.K. Zhang, J. Chu, X.Q. Wang, R.L. Zhang, M. Gong, B.H. Wu, Hydrothermal synthesis of porous sugarcane bagasse carbon/MnO2nanocomposite for supercapacitor application, J. Electron. Mater. 47 (2018) 6575–6582.

[31] Y. Zhu, T. Fang, J. Hua, S. Qiu, H. Chu, Y. Zou, C. Xiang, P. Huang, K. Zhang, X. Lin, E. Yan, H. Zhang, F. Xu, L. Sun, J.L. Zeng, Biomass-derived porous carbon prepared from egg white for high-performance supercapacitor electrode materials, Chemistry Select 4 (2019) 7358–7365.

[32] T. Mitravinda, K. Nanaji, S. Anandan, A. Jyothirmayi, V.S.K. Chakravadhanula, C.S. Sharma, T.N. Rao, Facile synthesis of corn silk derived nanoporous carbon for an improved supercapacitor performance, J. Electrochem. Soc. 165 (2018) A3369–A3379.

[33] C. Yuan, H. Lin, H. Lu, E. Xing, Y. Zhang, B. Xie, Synthesis of hierarchically porous MnO2/rice husks derived carbon composite as high-performance electrode material for supercapacitors, Appl. Energy 178 (2016) 260–268.

[34] J. Liu, H. Li, H. Zhang, Q. Liu, R. Li, B. Li, J. Wang, Three-dimensional hierarchical and interconnected honeycomb-like porous carbon derived from pomelo peel for high performance supercapacitors, J. Solid State Chem257 (2018) 64–71.

[35] W.L. Zhang, J.H. Xu, D.X. Hou, J. Yin, D.B. Liu, Y.P. He, H.B. Lin, Hierarchical porous carbon prepared from biomass through a facile method for supercapacitor applications, J. Colloid Interface Sci. 530 (2018) 338–344.

[36] J. Li, Q.M. Yang, I. Zhitomirsky, Composite electrodes for electrochemical supercapacitors, Nanoscale Res. Lett. 5 (2010) 512–517.

[37] J. Yao, Q. Pan, S. Yao, L. Duan, J. Liu, Mesoporous MnO2nanosphere/graphene sheets as electrodes for supercapacitor synthesized by a simple and inexpensive reflux reaction, Electrochim Acta238 (2017) 30–35.

[38] H. Wang, P. Cheng, P. Feng, H. Yu, J. Yang, Facile synthesis of MnO2/CNT nanocomposite and its electrochemical performance for supercapacitors, Mater. Sci. Eng. B 176 (2011) 1073–1078.

[39] A. Zolfaghari, H.R. Naderi, H.R. Mortaheb, Carbon black/manganese dioxide composites synthesized by sonochemistry method for electrochemical supercapacitors, J. Electroanal. Chem. 697 (2013) 60–67.

[40] Y. Peng, C. Zheng, W. Jing, Q. Xiao, W. Ding, S. He, H. Geng, Y. Lu, Hierarchical manganese oxide/carbon nanocomposites for supercapacitor electrodes, Nano Res. 4 (2011) 216–225.

[41] Z. Dong, H. Wang, M. Nan, Y. Chen, Z. Ying, T. Yin, X. Hui, L. Wei, S. Chen, W. Xin, High energy supercapacitors based on interconnected porous carbon nanosheets with ionic liquid electrolyte, Microporous Mesoporous Mater. 241 (2017) 202–209.